Available online at www.sciencedirect.com
ScienceDirect
Aerosol Science 39 (2008) 99–112
Journal of Aerosol Science
www.elsevier.com/locate/jaerosci

Towards quantitative prediction of aerosol deposition from turbulent flows

Simon Parker*, Timothy Foat, Steve Preston

Dstl, Porton Down, Salisbury, Wiltshire SP4 0JQ, UK

Received 28 July 2006; received in revised form 7 October 2007; accepted 9 October 2007

Abstract

Predictions of aerosol deposition rates from turbulent flow using computational fluid dynamics simulations have been compared with experimental data. The influence of turbulence model choice has been assessed. The use of isotropic turbulence models resulted in over-prediction of V_+ by more than 3 orders of magnitude for $\tau_+ \sim 0.2$, whilst the anisotropic RSM gave results in good agreement with experiment. For $\tau_+ > 10$ ($d_p \sim 10\,\mu m$ for $Re = 9894$) there was little difference between the turbulence models. Simulations for both $Re = 9894$ and 50,000 were carried out and good performance was seen for both. The effect of drag model was assessed and resulted in little difference in predicted deposition velocity. The influence of grid resolution was also investigated and it was seen that the cell centre of the wall-adjacent cell should be at a distance of $y_+ = 2$ or less for quantitative prediction of deposition. Coarser grids resulted in over-prediction for low τ_+.
Crown Copyright © 2007 Published by Elsevier Ltd. All rights reserved.

Keywords: Aerosol deposition; Computational fluid dynamics; Modelling; Pipe flow; Turbulence model

1. Introduction

Aerosol deposition is a problem of relevance both industrially and scientifically. It can be the cause of significant losses during transmission of aerosols through sampling lines and collection inlets. Aerosol deposition is an important consideration for the efficient delivery of therapeutic agents via the respiratory tract (Matida, DeHann, Finlay, & Lange, 2003). The deposition of aerosols is also of practical consequence for the nuclear industry (Gupta & McFarland, 2001).

Experimental studies of deposition from turbulent flow have been carried out by many authors including Friedlander and Johnstone (1957), Liu and Agarwal (1974) and McCoy and Hanratty (1977). A review of the subject can be found in Papavergos and Hedley (1984).

Whilst there is empirical deposition data available for flow in a straight pipe (Lee & Gieseke, 1994; Liu & Agarwal, 1974; Papavergos & Hedley, 1984), ducts (Zhang & Ahmadi, 2000) and for pipe bends (Pui, Romay-Novas, & Liu, 1987), there is a need to estimate turbulent deposition for non-regular geometries. Computational fluid dynamics (CFD) modelling is a technique routinely used to assess air flows and aerosol trajectories. It is also possible to use such techniques to estimate particle deposition from turbulent flows (Matida et al., 2003; Matida, Finlay, Lange, & Grgic, 2004; Nowak, Kakade, & Annapragada, 2003; Sarangapani & Wexler, 2000; Stapleton, Guentsch, Hoskinson,

* Corresponding author. Tel.: +44 1980 613266; fax: +44 1980 613987.
E-mail address: stparker@dstl.gov.uk (S. Parker).

0021-8502/$ - see front matter Crown Copyright © 2007 Published by Elsevier Ltd. All rights reserved.
doi:10.1016/j.jaerosci.2007.10.002

& Finlay, 2000; Zhang, Finlay, & Matida, 2004). However, the amount of deposition predicted has been seen to depend on the details of the particle tracking algorithm used (Matida et al., 2004). In particular, the use of isotropic turbulence models without near-wall corrections can result in significant over-prediction of deposition (Matida et al., 2003, 2004; Zhang et al., 2004). Because of the complex nature of the geometries considered in the above works, it is difficult to establish the underlying reason for poor model performance where it occurs. This work differs from those above in that it treats a simple straight pipe geometry for which experimental data are available. A systematic study of the dependence of CFD model results on the choice of turbulence model and grid resolution in a simple geometry has been carried out in order to provide a better understanding of the requirements for quantitative predictions. This work includes the use of the less commonly applied Reynolds stress model (RSM) for turbulence, which predicts the near-wall turbulent stresses in sufficient detail to model aerosol deposition with greater accuracy than two equation turbulence models.

In order to use CFD-based simulations with confidence it is necessary to establish their dependence on the modelling approach used. The intention of this work is to clearly define the behaviour of such simulations when used for practical aerosol deposition problems. To test the applicability of this type of model, predicted deposition has been compared with published experimental data for turbulent deposition from a flow within a vertical straight pipe (Liu & Agarwal, 1974). A systematic study of the influence of turbulence model, Reynolds number, drag law and the near-wall resolution has been carried out.

2. Particle deposition mechanisms

In the absence of electrostatic and gravitational forces, the deposition of particles of diameter greater than approximately 1 μm is largely the result of inertial effects (Lee & Gieseke, 1994). For smaller particle sizes, Brownian motion becomes an important mechanism. The process of aerosol deposition from turbulent flow has been represented by a number of authors as a two-stage process (Papavergos & Hedley, 1984). The first stage involves transport within the core turbulent region of the flow. In this stage the aerosol is readily moved normal to the mean flow direction by turbulent eddies, resulting in an approximately uniform concentration profile in the core of the flow, normal to the direction of flow. In the second stage the aerosol reaches the viscous sub-layer close to the wall where mean and turbulent velocities are lower. In particular, the wall-normal component of the turbulence is lower than the streamwise component close to the wall (Kim, Moin, & Moser, 1987). The transport of an aerosol across this region will depend on its inertia as it enters this region and also its rate of diffusion. Particles with sufficient inertia can cross to the wall and deposit and the rate of deposition depends strongly on particle relaxation time. This ‘free-flight’ picture has been updated by Botto, Narayanan, Fulgosi, and Lakehal (2005) who suggest that high concentrations close to the wall make the rate of deposition sensitive to near-wall turbulence and diffusion, even for larger particles. In order to correctly simulate aerosol deposition and the variation in behaviour with particle diameter it is important to capture the inertial behaviour of the aerosol and the variation in turbulent properties of the flow close to the wall.

The amount of deposition from a turbulent flow can be described by a deposition velocity V defined as

$$V = \frac{F}{C}, \tag{1}$$

where F is the flux of aerosol to the surface and C is the airborne concentration of the aerosol. The deposition velocity has been shown to depend on the particle relaxation time, τ:

$$\tau = \frac{\rho_p d_p^2 C_c}{18\mu}, \tag{2}$$

where ρ_p is the particle density, d_p is the particle diameter, C_c is the Cunningham slip correction factor and μ is the dynamic fluid viscosity. For deposition from a turbulent flow these numbers can be made non-dimensional using the friction velocity and kinematic fluid viscosity as follows:

$$V_+ = \frac{V}{u_*} \tag{3}$$

and

$$\tau_+ = \tau \frac{u_*^2}{\nu}, \tag{4}$$

where ν is the kinematic fluid viscosity and u_* is the friction velocity defined as

$$u_* = \sqrt{\frac{\tau_w}{\rho_f}}, \tag{5}$$

where τ_w is the wall shear stress and ρ_f is the fluid density.

When the deposition velocity and the particle relaxation time are made non-dimensional, a correlation is seen for turbulent pipe flow as described by a number of authors, for example, Lee and Gieseke (1994), Liu and Agarwal (1974) and Papavergos and Hedley (1984). For dimensionless relaxation times between 0.1 and 10, deposition varies strongly with particle diameter (Liu & Agarwal, 1974). This regime is important for the practical sampling of aerosols and it is therefore vital to understand the variation in deposition for aerosol-flow combinations in this range. This inertial range has been assessed in this paper and the deposition of smaller particles, dominated by Brownian diffusion, has not been considered.

3. Computational fluid dynamics

The use of CFD for predicting the properties of fluid systems has been described in detail elsewhere. The unfamiliar reader is directed to Versteeg and Malalasekera (1995). However, the treatment of turbulent flows with CFD deserves particular mention. The large range of spatial and temporal scales of turbulent eddies requires extremely large computational resources to simulate them directly. As a result, models of turbulence are used in combination with Reynolds averaged Navier–Stokes equations to predict the time-averaged properties of turbulent flows for practical applications. Turbulence models can be divided into two types: isotropic which makes no distinction between the spatial components of the turbulence and anisotropic which differentiates between the spatial components. The specific turbulence models used in this study are discussed further below.

For the aerosol concentrations considered in this work the aerosol can be considered as dilute, with one-way coupling between the fluid and aerosol. The aerosol particle volume fractions in the experiments against which the model results are compared were estimated to be less than 10^{-7}. For such low volume fractions Elghobashi (1994) suggests that the aerosols have a negligible effect on turbulence and measurements by Rashidi, Hetsroni, and Banerjee (1990) have shown that they have no effect on the rate of turbulent wall ejections. For the simulation of a dilute aerosol flow, the solution of the fluid flow can be performed prior to the simulation of the aerosol behaviour using a Lagrangian approach. The trajectory of an aerosol can be calculated from its starting position and the forces acting upon it. A general particle force balance equation in one direction can be written as (Fluent Inc., 2005)

$$\frac{du_p}{dt} = F_D(u_f - u_p) + g_x \frac{(\rho_p - \rho_f)}{\rho_p} + F_x, \tag{6}$$

where u_p is the velocity of the particle, u_f is the fluid velocity, F_D is the force per unit mass due to fluid drag, g_x is the gravitational acceleration in the considered direction, ρ_p is the particle density and F_x is the sum of other forces such as those due to Brownian motion and Saffman lift force.

The trajectory of an individual particle in a turbulent flow will depend on the local instantaneous fluid velocity that it experiences. However, in the case of a Reynolds averaged Navier–Stokes solution such information is not available directly. The eddy-interaction approach (Graham & James, 1996) recreates a series of eddies based on the statistical turbulent properties of the flow. Each particle experiences a velocity based on a random number sampled from a Gaussian distribution, scaled by the RMS of the fluctuating velocity component. For the isotropic models, each direction is scaled by the same factor, whereas for the non-isotropic turbulence models each direction is scaled independently. The timescale of the interaction with each eddy is determined by an eddy lifetime scaled by the turbulent kinetic energy and dissipation rate and an eddy crossing time (Fluent Inc., 2005). Deposition is determined by the intersection of the particle trajectory with the walls of the domain.

4. Methodology

4.1. Validation data

The experimental work of Liu and Agarwal (1974) was chosen as a test case for CFD simulation because it is widely quoted and provides sufficient details to allow a model to be created. The experiment involved the measurement of deposition of sodium fluorescein tagged olive oil aerosol in a vertical straight glass pipe of internal diameter 0.0127 m for two different Reynolds numbers ($Re = 9894$ and 50,000). The authors divided the pipe into eight sections and reported the mass of deposited aerosol to each section for a range of aerosol diameters. Based on these measurements the dimensionless deposition velocity for each aerosol dimensionless relaxation time was reported.

A CFD simulation of the air flow through the pipe used in the experiment was carried out using the Fluent® software, v.6.2.16. The pipe length was 1.02 m and the internal diameter was 0.0127 m. Two volumetric flow rates were considered $1.5 \times 10^{-3}\,\mathrm{m^3\,s^{-1}}$ ($Re = 9894$) and $7.6 \times 10^{-3}\,\mathrm{m^3\,s^{-1}}$ ($Re = 50,000$).

A two-dimensional axi-symmetric model of the straight pipe was created. The resolution of the boundary layer adjacent to the pipe was chosen to be of sufficient resolution to resolve the viscous sub-layer and the enhanced wall treatment option was used in the CFD code. The centre of the cell closest to the wall was chosen to be at a non-dimensional distance of $y_+ = 1$, based on the recommendations for the enhanced wall functions boundary conditions (Fluent Inc., 2005). y_+ was calculated using the following formula:

$$y_+ = y\left(\frac{u_*}{\nu}\right), \tag{7}$$

where y is the wall-normal distance. The friction velocity, u_*, was calculated, following Liu and Agarwal (1974), using

$$u_* = \left(\frac{f}{2}\right)^{1/2}\bar{u}, \tag{8}$$

where $\bar{u}$ is the mean fluid velocity and f is the friction factor for the pipe. The friction factor was calculated, following Liu and Agarwal (1974), for a smooth pipe:

$$f = \frac{0.316}{4(Re)^{1/4}}, \tag{9}$$

where Re is the flow Reynolds number. For the simulated pipe with $Re = 9894$, $u_* = 0.745\,\mathrm{m\,s^{-1}}$ and $y = 0.02$ mm when $y_+ = 1$, whilst, for $Re = 50,000$, $u_* = 3.08\,\mathrm{ms^{-1}}$ and $y = 0.005$ mm when $y_+ = 1$. The u_* value calculated by the CFD simulation agreed with these values to within 10%.

The size of the cells in the direction normal to the wall was set to increase geometrically by a factor of 1.1. The length of the cells in the direction parallel to the pipe axis was 0.5 mm, giving a maximum aspect ratio of 12 for the wall-adjacent cells for $Re = 9894$ and 50 for $Re = 50,000$.

4.2. Boundary conditions

The boundary conditions for the flow consisted of a no-slip wall for the pipe wall. The roughness of the wall can influence particle deposition (Chamberlain, Garland, & Wells, 1984; Lai, Byrne, & Goddard, 1999, 2001; Schack, Pratsinis, & Friedlander, 1985) and affects the velocity profile within the boundary layer. The experiments of Liu and Agarwal (1974) used glass pipes and for the purposes of the simulations it has been assumed that the wall was smooth. The centreline of the pipe was defined as an axis of symmetry. The inlet to the pipe was defined with a uniform velocity oriented along the pipe axis with no variation in velocity with radial position. The velocity inlet was specified with 10% turbulence intensity and a hydraulic diameter equal to the pipe diameter. Whilst this is a simplification, a more detailed specification is not appropriate since the pipe begins at a tee-piece in the experiment, the details of which are not provided. A steady velocity and turbulence profile was established within a relatively short length of the pipe from the inlet and only the final half of the pipe was used to calculate aerosol deposition. Therefore, the influence of the velocity and turbulence conditions at the inlet has a small effect on the predicted deposition. The outlet to the pipe was defined as an outflow condition. The orientation of the pipe was vertical with the flow oriented downwards. Whilst

gravity and lift force can increase the deposition velocity in a downwards vertical flow, Zhang and Ahmadi (2000) predicted that the effect decreases with friction velocity, quoting a value of a 10% increase for $u_* = 0.3\,\mathrm{m\,s^{-1}}$. For $u_* \geqslant 0.745\,\mathrm{m\,s^{-1}}$ considered in this study, the effects of gravity and lift force will have a small effect and have been neglected.

4.3. Solver settings

The air flow through the pipe was solved using a segregated steady-state Reynolds averaged Navier–Stokes solver. Discretisation of the equations was set to second order. The solution was iterated until the residual error in the equations had been minimised and reached a steady value.

4.4. Aerosol tracking

Following the solution of the air flow through the pipe the trajectories of different sized aerosol particles were calculated. It was assumed that the aerosol particles were sufficiently dilute that they had no significant influence on each other or the air flow through the pipe. The discrete random walk (DRW) model (Fluent Inc., 2005) was used to simulate the particle trajectories as described above. The maximum number of particle steps for a single trajectory was set to 10^6, and the integration steps were adjusted dynamically to approximately five steps within each computational cell. For each simulation a total of between 4×10^4 and 4×10^6 particles were tracked.

On reaching the wall the particles were considered to be trapped with zero probability of bounce. This is a reasonable assumption for the olive oil particles used in the experiment. Once deposited, particles were also assumed to have a zero probability of resuspension. Electrostatic forces can also have a significant effect on particle motion and deposition. The charges on the particles in the experiment used for comparison were neutralised following their production and, therefore, electrostatic forces have been neglected in this study. Force due to gravity and lift force were not included because of the vertical orientation of the pipe and the high value of u_* as discussed above. Brownian motion and thermophoresis were not included in the simulation. Tests showed that these forces were of less influence than the other variables assessed.

The aerosols were defined with an initial velocity equal to the mean fluid velocity. The density of the particles was set to $920\,\mathrm{kg\,m^{-3}}$ to represent olive oil, as used in the experiments of Liu and Agarwal (1974). For $Re = 9894$, the particle diameter varied from 1 μm ($\tau_+ = 0.12$) to 100 μm ($\tau_+ \sim 1020$) and for $Re = 50,000$ it varied from 0.2 μm ($\tau_+ = 0.13$) to 20 μm ($\tau_+ \sim 704$) For each particle diameter studied, 40 initial locations across the radius of the pipe inlet were used. The initial locations had a higher density towards the outside of the pipe since the radial spacing of these positions in two dimensions was arranged so that, when extrapolated to three dimensions, each release occupied an equal area of the pipe inlet.

4.5. Deposition velocity calculation

The rate of aerosol deposition was calculated for each of eight sequential and equal length sections of the pipe, as measured in the experiment of Liu and Agarwal (1974). Only the data for the downstream four sections of pipe were used to ensure that the flow and aerosol distribution were fully developed in the pipe. Using these data the deposition velocity was calculated for each particle size. The non-dimensional deposition velocity and relaxation time were calculated for each particle size using Eqs. (3) and (4) above.

Because of the stochastic nature of the aerosol deposition calculations it is useful to estimate the uncertainty in the calculated values. The deposition to any one section of the pipe can be considered as a Monte-Carlo process, with a probability of deposition p_d. For such a process, the uncertainty can be estimated from the following equation (Bevington & Robinson, 2003):

$$\sigma = \sqrt{N_\mathrm{d}(1 - p_\mathrm{d})}, \tag{10}$$

where σ is the uncertainty in the number of deposited particles, N_d is the number of particles deposited and p_d is the probability of the particles depositing. Note that both σ and p_d are strictly estimates, since their calculation is based on the deposition from a finite number of stochastically tracked particles. Using this relationship, the uncertainties in

the number of particles deposited in each section and in the dimensionless deposition velocity were calculated and are plotted as error bars on the graphs in Fig. 4–8. Stochastic simulations of aerosol trajectories can be computationally expensive because of the large number of particles that needs to be tracked. Eq. (10) allows some estimate to be made of the number of trajectories needed and can save considerable time in such calculations.

4.6. Turbulence modelling

As discussed above, the behaviour of turbulence is important in determining aerosol deposition. To assess the effect of turbulence models used in CFD calculations, three different turbulence models were compared. Two isotropic turbulence models, the renormalisation group k–ε model (RNG) and the k–ω shear stress transport (SST) model, and an anisotropic turbulence model, the RSM, were used. All three models are widely used engineering turbulence models, although the k–ε model is perhaps the most popular. Both the k–ε and k–ω model have been used by a number of authors to study aerosol deposition (Matida et al., 2004; Zhang et al., 2004). The isotropic models are less computationally expensive than the RSM approach, requiring only two equations compared with the seven needed for the RSM in a three-dimensional calculation. Both the RNG and RSM were used with enhanced wall functions, with the exception of the coarse resolution models described below. This approach blends the laminar and turbulent wall functions depending on the distance from the wall (Fluent Inc., 2005). The SST model uses a similar approach by default. The boundary conditions for the RSM were calculated from the turbulent kinetic energy. Wall reflection effects were included in the RSM formulation which contribute to the damping of the wall-normal stresses and enhancement of stresses parallel to the wall.

4.7. Reynolds number

The comparisons for the turbulence models were carried out using the simulated pipe flow with a Reynolds number of 9894. To assess the performance of CFD predictions under different conditions, a pipe flow with a Reynolds number of 50,000 was also simulated for comparison with the other flow condition reported by Liu and Agarwal (1974). The remaining simulations described below were all run with a Reynolds number of 9894.

4.8. Drag model

The effect of the variation of drag model was assessed by comparing the Stokes–Cunningham model, the spherical drag model of Morsi and Alexander (1972) and the non-spherical drag model of Haider and Levenspiel (1989). The spherical and non-spherical models are incorporated into the Fluent software and the value for the Stokes–Cunningham correction factor was calculated using a user-defined function following Hinds (1999). For the non-spherical model three different sphericity values were compared: 1, 0.872 and 0.806. The value of 1 represents a spherical particle for comparison with other two drag models. The value of 0.872 was chosen to represent the sphericity of a bacterial spore, based on a cylindrical shape, with hemispherical ends. A length of 1.8 μm and a width of 0.7 μm were used as typical values for *Bacillus subtilis* subsp. *niger*. (Johnson, Martin, & Resnick, 1994), a common bacterial stimulant used for biological aerosol testing, to calculate the relative dimensions and sphericity of 0.872. The sphericity value of 0.806 represents cubic shapes (Haider & Levenspiel, 1989) as is typical of some crystalline aerosols such as sodium chloride. These models were compared using the Reynolds stress turbulence model and the case of $Re = 9894$.

4.9. Mesh resolution

The influence of the resolution of the mesh used to divide the geometry into finite volumes was also examined. The best performing turbulence model was used to simulate the flow and aerosol deposition using meshes with varying height of the wall-adjacent cell. Two main approaches to the treatment of wall boundaries are possible within the CFD code used. Because of the importance of the viscous sub-layer in controlling the rate of deposition, it was expected that the explicit modelling of this layer would be required in order to achieve quantitative predictions of deposition. The enhanced wall treatment approach is designed to resolve the boundary layer down through the viscous sub-layer and is based on a function suggested by Kader (1981). The y_+ for the wall-adjacent cell centre for such treatment is recommended to be of the order of 1 (Fluent Inc., 2005). The cell centre height was varied from a value of $y_+ = 1$ to

Table 1
Grid sensitivity cases using RSM for $Re = 9894$

Model code	Wall function	Cell centre y_+ for wall-adjacent cell	Cell height growth factor	Number of radial cells	Total number of cells
Y1	Enhanced	1	1.1	29	59,160
Y2	Enhanced	2	1.1	20	40,800
Y3	Enhanced	3	1.1	18	36,720
Y5	Enhanced	5	1.1	14	28,560
Y10	Enhanced	10	1.1	10	20,400
Y10_SWF	Standard	10	1.1	10	20,400
Y20_SWF	Standard	20	1.1	7	14,280
Y30_SWF	Standard	30	1.1	4	8160
Y60_SWF	Standard	60	1.1	3	6120

10 to explore the consequences of coarsening the mesh in practical CFD problems. In many engineering applications of CFD it is not always possible to control the y_+ value with a high degree of accuracy, without knowledge of the flow field in advance. As a result it is important to consider what effect such differences in the y_+ value of the wall-adjacent cell may have.

The performance of models using standard wall functions was also assessed. The standard wall functions are based on the approach of Launder and Spalding (1974). A y_+ value of 30 is recommended for such wall functions, and values of y_+ between 5 and 30 are not recommended. However, as discussed above, in practical CFD problems with complex geometries, where the flow field cannot be predicted easily, it is not always possible to prescribe the y_+ value for all wall-adjacent cells. Values of y_+ of 10, 20, 30 and 60 were therefore examined. The cell spacing was increased away from the wall using a ratio of 1.1 for all of the models. It was expected that a standard wall function approach would be too coarse to accurately capture the wall-deposition process. However, these cases were included to demonstrate the inadequacy of such an approach and highlight the degree of error that can be introduced by using such coarse meshes and default wall function approaches. Table 1 summarises the different grid sensitivity cases modelled.

5. Results and discussion

5.1. Flow properties

The calculated mean streamwise velocity field was very similar for each of the turbulence models. Fig. 1 shows the normalised streamwise velocity, u_+ (defined as u/u_*), midway along the pipe for each model for $Re = 9894$. The experimental data of Durst, Jovanovic, and Sender (1995) measured using laser Doppler anemometry within a pipe flow of $Re = 7442$ are included for comparison. The profile is very similar between the three turbulence models and the experimental data, with only a small relative increase in the centreline velocity predicted by the k–ω SST model relative to the other models. Fig. 2 shows the profiles of the three different spatial components of the turbulence calculated by the RSM. The root mean square velocities ($u' = \sqrt{\overline{u^2}}$) for each direction are presented, normalised by the friction velocity ($u'_+ = u'/u_*$). The damping of the wall-normal stress (v') is clear close to the wall. Experimental measurements from Durst et al. (1995) of turbulent pipe flow at $Re = 7442$ and 13,500 are included for comparison. The predicted streamwise turbulence component appears to match well with the experimental data, whilst the wall-normal and lateral components are slightly under-predicted.

For the isotropic turbulence models the magnitude of the wall-normal stress (v') and the streamwise (u') and lateral (w') components are calculated from the turbulent kinetic energy, k (Fluent Inc., 2005):

$$\sqrt{\overline{u'^2}} = \sqrt{\overline{v'^2}} = \sqrt{\overline{w'^2}} = \sqrt{\frac{2k}{3}}. \tag{11}$$

Fig. 3 shows the wall-normal stress for each of the turbulence models and experimental data for comparison. The importance of the damping due to the presence of the wall is clear for the region $y_+ < 50$. There is also a significant

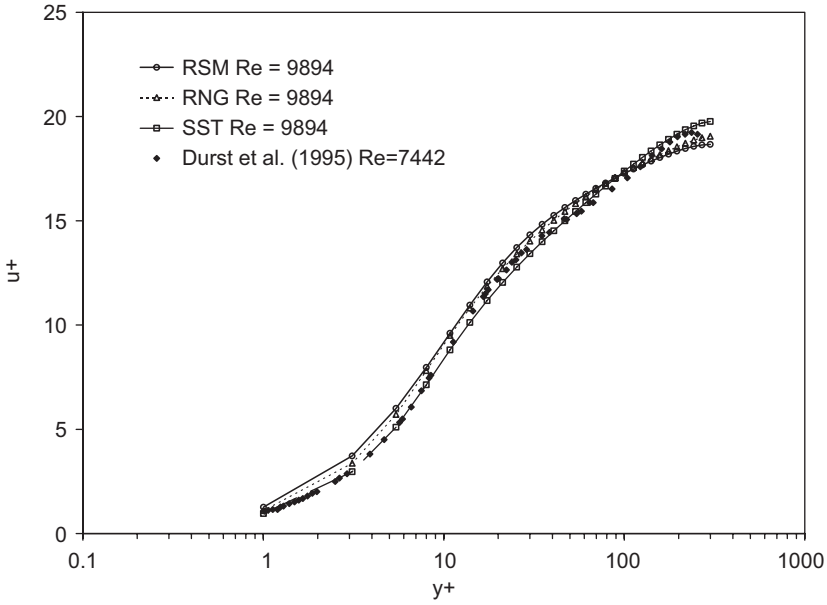

Fig. 1. Axial velocity against wall distance plotted radially at half the streamwise distance along the pipe, as predicted by three turbulence models ($Re = 9894$) and measured by Durst, Jovanovic, and Sender (1995) ($Re = 7442$). RSM—Reynolds stress model, RNG—renormalisation group $k - \varepsilon$ model, and SST—shear stress transport k–ω model.

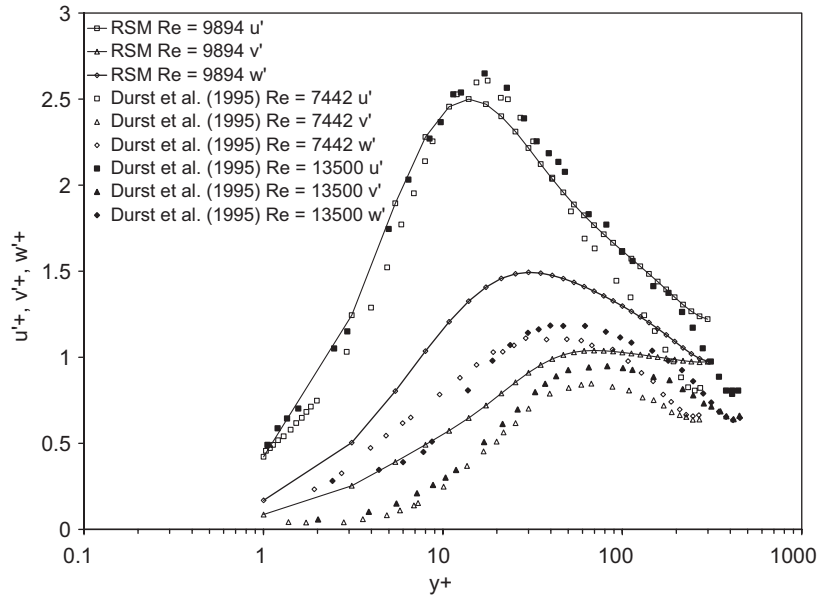

Fig. 2. Three components of turbulent stress predicted by Reynolds stress model ($Re = 9894$), plotted radially at half the streamwise distance along the pipe. u'_+—streamwise, v'_+—wall-normal and w'_+—lateral stress. Measured stresses from Durst et al. (1995) ($Re = 7442$ and $13,500$).

difference between the RNG k–ε model and the SST k–ω model, with the RNG model predicting higher values for the wall-normal stress than the SST model. All three turbulence models over-predict the wall-normal turbulence; however, the RSM is the closest to the observed values.

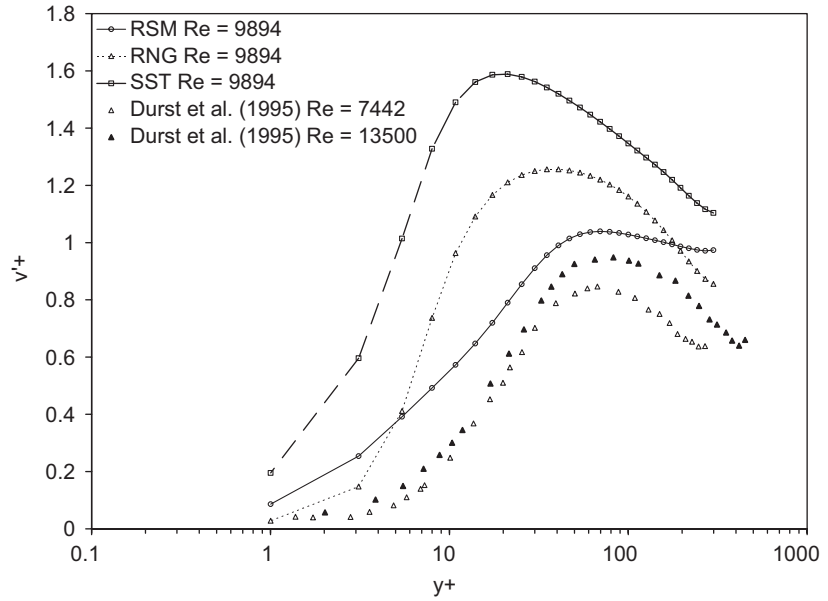

Fig. 3. Wall-normal component of turbulent stress predicted by three different turbulence models, plotted radially at half the streamwise distance along the pipe, computed for $Re = 9894$. RSM—Reynolds stress model, RNG—renormalisation group k–ε model and SST—shear stress transport k–ω model. Measured stresses from Durst et al. (1995) ($Re = 7442$ and 13,500).

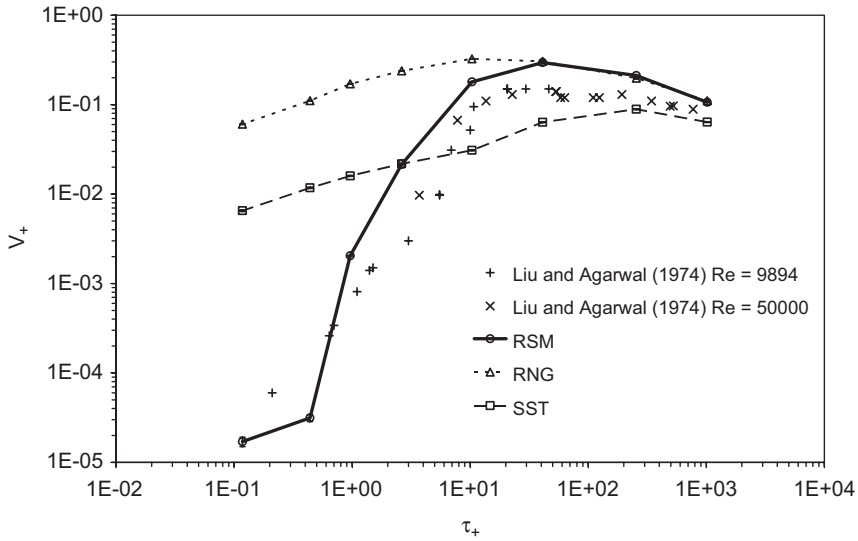

Fig. 4. Dimensionless deposition velocity against dimensionless particle relaxation time for three different turbulence models simulating flow for $Re = 9894$, $y_+ = 1$. RSM—Reynolds stress model, RNG—Renormalisation group k–ε model and SST—shear stress transport k–ω model. Error bars show estimated uncertainty. Experimental data from Liu and Agarwal (1974) for $Re = 9894$ and 50,000.

5.2. Deposition dependence on turbulence model

The variation in predicted dimensionless deposition velocity with particle dimensionless relaxation time is shown in Fig. 4 for each of the three turbulence models. The experimental data of Liu and Agarwal (1974) for both Reynolds numbers are also shown on this plot. There is a striking difference in the results produced by the three turbulence

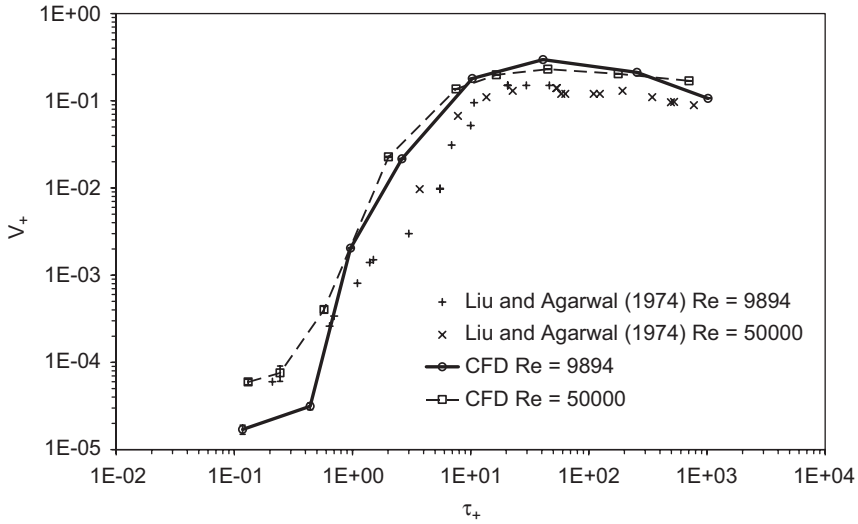

Fig. 5. Dimensionless deposition velocity against dimensionless particle relaxation time using RSM, $y_+ = 1$ for $Re = 9894$ and 50,000. Error bars show estimated uncertainty. Experimental data from Liu and Agarwal (1974) for $Re = 9894$ and 50,000.

models. For $10 < \tau_+ < 1000$ (approximately 10 μm $< d_p <$ 100 μm for $Re = 9894$) all three turbulence models perform reasonably well, predicting a dimensionless deposition velocity within approximately a factor of 2 of the experimental data. However, for $\tau_+ < 10$ ($d_p \sim 10$ μm for $Re = 9894$) the experimental deposition velocity varies very strongly with the relaxation time. Neither of the two isotropic turbulence models captures this behaviour and both over-predict the deposition velocity at small relaxation times by 2–3 orders of magnitude. The anisotropic RSM performs much better, capturing the strong relaxation time dependence in this region, although it does over-predict the deposition velocity slightly. This over-prediction may be due to the slight over-prediction of wall-normal stresses as shown in Fig. 3. The uncertainty in the predicted deposition velocity for the RSM becomes noticeable for the smallest dimensionless deposition velocities, but is small compared to the variation between models and between model and experiment.

The relative over-prediction of deposition by the isotropic turbulence models can be explained by considering the higher wall-normal stresses for these models than the anisotropic model in Fig. 3. The RNG k–ε model which predicts the greatest amount of deposition also shows the greatest wall-normal stress close to the wall. The inability of these turbulence models to capture the damping of the wall-normal stresses close to the wall is believed to be the cause of their over-prediction of the aerosol deposition.

The over-prediction of deposition seen for the isotropic turbulence models agrees with the experience of other workers using these models for more complicated geometries (Matida et al., 2003, 2004; Stapleton et al., 2000; Zhang et al., 2004). Corrections to the near-wall turbulence profiles have been implemented for isotropic models to correct for this over-prediction (Matida et al., 2003; Wang & James, 1999) and can provide a computationally less expensive approach. However, the corrected approach is strictly only applicable to fully developed flows and may therefore be less suitable than a fully anisotropic model for complex geometries. The focus of this work was to examine techniques which can be applied to a range of flows in complex geometries and has not included an assessment of such corrections. It should also be noted that although the solution time for the flow will be longer with the RSM than for an isotropic model, the particle tracking stage, which can be a considerable part of the overall solution time, should be turbulence model independent.

5.3. Reynolds number dependence

It is clear that, of the three turbulence models considered, the RSM is significantly better at predicting the variation in deposition velocity with particle relaxation time. The RSM was used for the remaining tests. Fig. 5 shows the results for the application of the RSM and a grid with wall-adjacent cell centre at $y_+ = 1$ for the same case as Fig. 4 ($Re = 9894$)

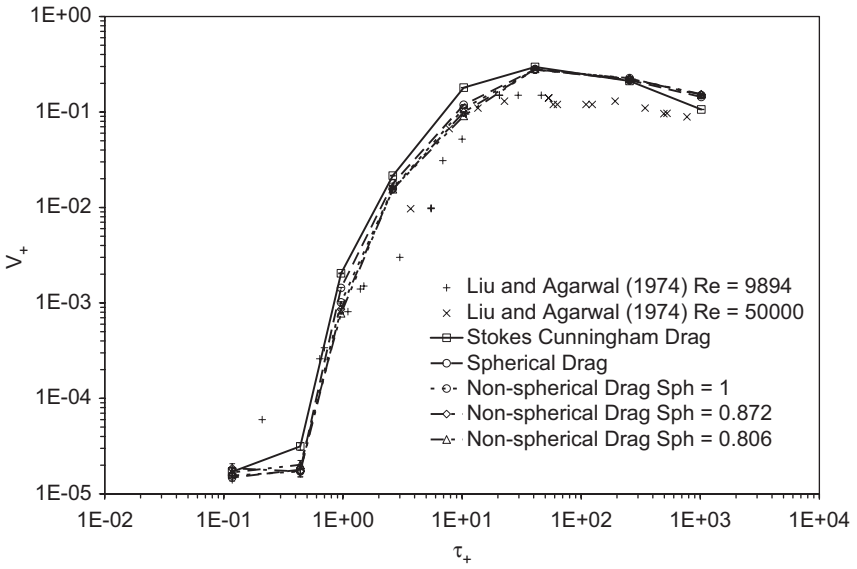

Fig. 6. Drag model influence on deposition velocity using RSM, $y_+ = 1$, computed for $Re = 9894$. Error bars show estimated uncertainty. Experimental data from Liu and Agarwal (1974) for $Re = 9894$ and 50,000.

and for the case of $Re = 50,000$. Both sets of data show very similar behaviour when made non-dimensional, showing a slight over-prediction at all but the smallest values of τ_+ tested.

5.4. Drag model dependence

Fig. 6 shows the results of the deposition velocity predicted using a range of drag models, simulating the flow at $Re = 9894$, with the RSM and a grid with wall-adjacent cell centre at $y_+ = 1$. There is little difference between the results, with the Stokes–Cunningham drag model showing slightly higher deposition velocities for $0.4 < \tau_+ < 10$. There is little difference to be seen between the three sphericity values used for the non-spherical drag approach.

5.5. Grid resolution dependence

For practical CFD simulations with more complex geometries it is often not possible to achieve optimum y_+ values throughout the domain. The dependence of the predicted deposition velocity on the grid resolution is shown in Figs. 7 and 8. Fig. 7 shows the performance with wall-adjacent cell centre y_+ values of 1–10 and enhanced wall treatment boundary conditions. Increasing the mesh size at the boundary resulted in increasing over-prediction of deposition for the smaller dimensionless relaxation times. There is also a slight reduction in the over-prediction at the peak in deposition velocity. There appears to be little to choose between $y_+ = 1$ and 2, although $y_+ = 2$ is a better fit to the experimental data at $\tau_+ = 0.21$.

Increasingly coarse meshes with $y_+ = 10$–60 were also used with standard wall functions since the enhanced wall treatment is not appropriate for such meshes. Fig. 8 shows the resulting deposition velocities in comparison to the experimental data of Liu and Agarwal (1974). For these coarser meshes the deposition velocity still shows a slight increase with increasing y_+ value for small relaxation times, but it is much less pronounced than for the smaller y_+ values. The performance at larger values of τ_+ is slightly better than for the finer computational meshes.

5.6. Implications

The results above indicate that it is possible to achieve quantitative estimates of aerosol deposition from dilute flows using a commercial CFD code. The use of a steady-state, sequential Eulerian–Lagrangian approach

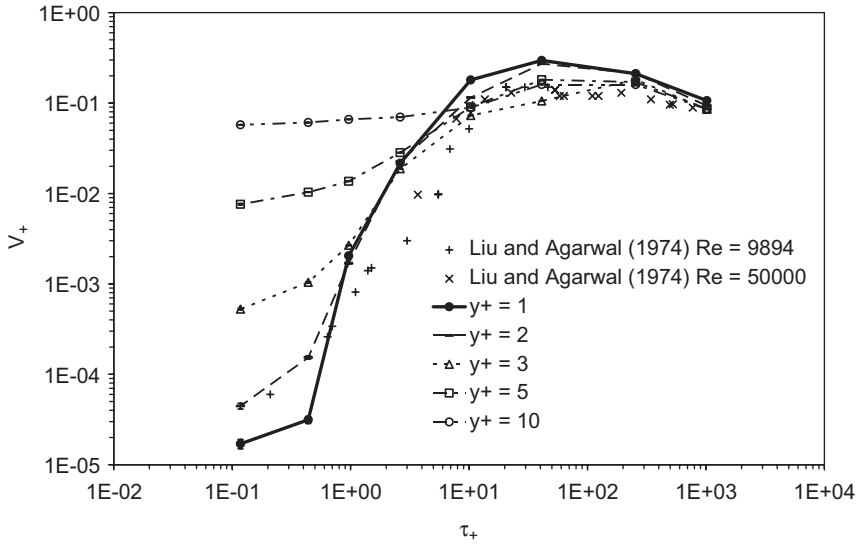

Fig. 7. Dimensionless deposition velocity against dimensionless particle relaxation time for different mesh resolutions using enhanced wall functions and RSM computed for $Re = 9894$. Error bars show estimated uncertainty. Experimental data from Liu and Agarwal (1974) for $Re = 9894$ and 50,000.

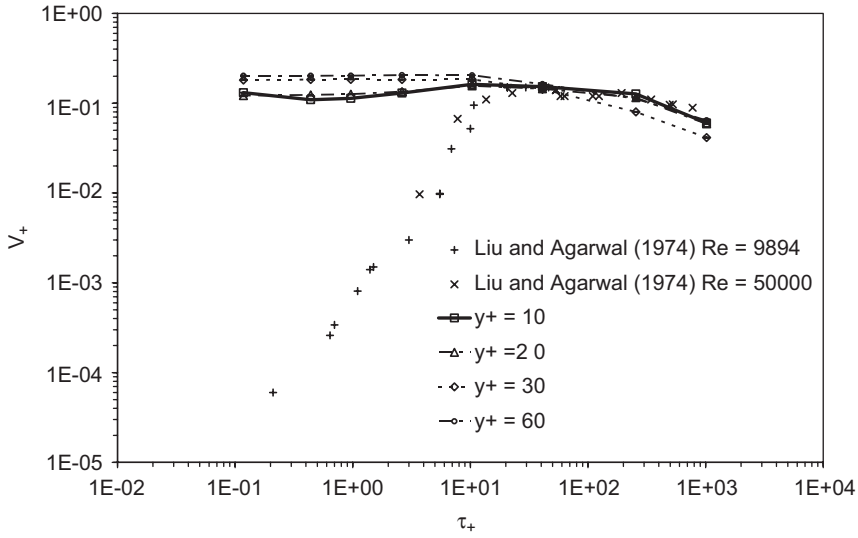

Fig. 8. Dimensionless deposition velocity against dimensionless particle relaxation time for different mesh resolutions using standard wall functions and RSM computed for $Re = 9894$. Error bars show estimated uncertainty. Experimental data from Liu and Agarwal (1974) for $Re = 9894$ and 50,000.

can provide dimensionless deposition velocities within an order of magnitude of experimental data, provided care is taken with the choice of modelling approach. In particular it has been shown that the accurate simulation of the near-wall turbulence by using anisotropic turbulence modelling and resolution of the viscous sub-layer is necessary to obtain correct results. Isotropic turbulence models over-estimate the wall-normal turbulence close to the wall resulting in over-estimates of deposition velocity. It is believed that insufficient resolution close to the wall prevents accurate capture of the slowing of aerosol trajectories as they approach the wall.

6. Conclusions

The ability of CFD models to predict aerosol deposition from turbulent flow in a straight vertical pipe has been assessed by comparison with experimental data (Liu & Agarwal, 1974). This study has limited itself to dilute aerosol flows and the use of steady-state Reynolds averaged Navier–Stokes models with turbulence modelling followed by Lagrangian particle tracking. However, the same approach could be used with an unsteady solution to the air flow.

Quantitative prediction of deposition was seen to rely on the use of an anisotropic turbulence model. Isotropic models, such as the k–ε and k–ω turbulence models, used without near-wall corrections were seen to over-predict deposition for small τ_+ ($d_p < 10\,\mu m$ for $Re = 9894$). This behaviour is believed to be due to the unrealistically high wall-normal turbulence components predicted close to the wall. Near-wall corrections (Matida et al., 2003; Wang & James, 1999) may be able to overcome this over-prediction and involve less computational expense than a full anisotropic approach. However, they may not be appropriate for complex geometries.

Using the anisotropic RSM for turbulence calculation, the two Reynolds numbers studied experimentally by Liu and Agarwal (1974) were simulated successfully. The simulations gave similar results for all but the smallest relaxation times studied.

The effect of three different models for the drag experienced by the aerosol particles was assessed including the consideration of non-sphericity. These models showed little difference in the results for the regime under study.

The effect of mesh resolution was also considered in some detail to explore the consequences of varying y_+ values in practical CFD simulations. For meshes with wall-adjacent cells with cell centre $y_+ > 2$ there was an increasing over-prediction of the deposition velocity with increasing cell size. These results suggest that the explicit modelling of the viscous sub-layer is required to capture the deceleration of aerosols approaching the wall.

An assessment of the uncertainty in the number of deposited particles from stochastic Lagrangian tracking results has been made using a simple relationship to the estimated deposition probability and the number of deposited particles.

In summary, quantitative predictions of aerosol deposition from dilute turbulent flow were achieved using CFD. An anisotropic turbulence model and sufficient near-wall grid resolution were both required to capture the correct variation of deposition velocity with $0.2 > \tau_+ > 10$. Based on these results, it is recommended that uncorrected isotropic turbulence models should not be used for aerosol deposition simulations for $\tau_+ < 10$.

Acknowledgements

This work has been supported by the United Kingdom Ministry of Defence. © Crown copyright 2007. Published with permission from the Defence Science and Technology Laboratory on behalf of the Controller of HMSO.

References

Bevington, P. R., & Robinson, D. K. (2003). *Data reduction and error analysis for the physical sciences*. New York: McGraw-Hill.

Botto, L., Narayanan, C., Fulgosi, M., & Lakehal, D. (2005). Effect of near-wall turbulence enhancement on the mechanism of particle deposition. *International Journal of Multiphase Flow*, *31*, 940–956.

Chamberlain, A. C., Garland, J. A., & Wells, A. C. (1984). Transport of gases and particles to surfaces with widely spaced roughness elements. *Boundary-Layer Meteorology*, *29*, 343–360.

Durst, F., Jovanovic, J., & Sender, J. (1995). LDA measurements in the near-wall region of a turbulent pipe-flow. *Journal of Fluid Mechanics*, *295*, 305–335.

Elghobashi, S. (1994). On predicting particle-laden turbulent flows. *Applied Scientific Research*, *52*, 309–329.

Fluent Inc. (2005). *Fluent 6.2.16 user's guide*. Lebanon: Fluent Inc.

Friedlander, S. K., & Johnstone, H. F. (1957). Deposition of suspended particles from turbulent gas streams. *Industrial and Engineering Chemistry*, *49*, 1151–1156.

Graham, D. I., & James, P. W. (1996). Turbulent dispersion of particles using eddy interaction models. *International Journal of Multiphase Flow*, *22*, 157–175.

Gupta, R., & McFarland, A. R. (2001). Experimental study of aerosol deposition in flow splitters with turbulent flow. *Aerosol Science and Technology*, *34*, 216–226.

Haider, A., & Levenspiel, O. (1989). Drag coefficient and terminal velocity of spherical and nonspherical particles. *Powder Technology*, *58*, 63–70.

Hinds, W. C. (1999). *Aerosol technology*. New York: Wiley.

Johnson, B., Martin, D. D., & Resnick, I. G. (1994). Efficacy of selected respiratory protective equipment challenged with *Bacillus subtilis* subsp. *niger*. *Applied and Environmental Microbiology*, *60*, 2184–2186.

Kader, B. (1981). Temperature and concentration profiles in fully turbulent boundary layers. *International Journal of Heat and Mass Transfer*, *24*, 1541–1544.

Kim, J., Moin, P., & Moser, R. (1987). Turbulence statistics in fully developed channel flow at low Reynolds number. *Journal of Fluid Mechanics*, *177*, 133–166.

Lai, A. C. K., Byrne, M. A., & Goddard, A. J. H. (1999). Measured deposition of aerosol particles on a two-dimensional ribbed surface in a turbulent duct flow. *Journal of Aerosol Science*, *30*, 1201–1214.

Lai, A. C. K., Byrne, M. A., & Goddard, A. J. H. (2001). Aerosol deposition in turbulent channel flow on a regular array of three-dimensional roughness elements. *Journal of Aerosol Science*, *32*, 121–137.

Launder, B. E., & Spalding, D. B. (1974). The numerical computation of turbulent flows. *Computer Methods in Applied Mechanics and Engineering*, *3*, 269–289.

Lee, K. W., & Gieseke, J. A. (1994). Deposition of particles in turbulent pipe flows. *Journal of Aerosol Science*, *25*, 699–709.

Liu, B. Y. H., & Agarwal, J. K. (1974). Experimental observation of aerosol deposition in turbulent flow. *Journal of Aerosol Science*, *5*, 145–155.

Matida, E. A., DeHann, W. H., Finlay, W. H., & Lange, C. F. (2003). Simulation of particle deposition in an idealized mouth with different small diameter inlets. *Aerosol Science and Technology*, *37*, 924–932.

Matida, E. A., Finlay, W. H., Lange, C. F., & Grgic, B. (2004). Improved numerical simulation of aerosol deposition in an idealized mouth–throat. *Journal of Aerosol Science*, *35*, 1–19.

McCoy, D. D., & Hanratty, T. J. (1977). Rate of deposition of droplets in annular two-phase flow. *International Journal of Multiphase Flow*, *3*, 319–331.

Morsi, S. A., & Alexander, A. J. (1972). An investigation of particle trajectories in two-phase flow systems. *Journal of Fluid Mechanics*, *55*, 193–208.

Nowak, N., Kakade, P. P., & Annapragada, A. V. (2003). Computational fluid dynamics simulation of airflow and aerosol deposition in human lungs. *Annals of Biomedical Engineering*, *31*, 374–390.

Papavergos, P. G., & Hedley, A. B. (1984). Particle deposition behaviour from turbulent flows. *Chemical Engineering Research and Design*, *62*, 275–295.

Pui, D. Y. H., Romay-Novas, F., & Liu, B. Y. H. (1987). Experimental study of particle deposition in bends of circular cross section. *Aerosol Science and Technology*, *7*, 301–315.

Rashidi, M., Hetsroni, G., & Banerjee, S. (1990). Particle–turbulence interaction in a boundary layer. *International Journal of Multiphase Flow*, *16*, 935–949.

Sarangapani, R., & Wexler, A. S. (2000). Modeling particle deposition in extrathoracic airways. *Aerosol Science and Technology*, *32*, 72–89.

Schack, C. J., Pratsinis, S. E., & Friedlander, S. K. (1985). A general correlation for deposition of suspended particles from turbulent gases to completely rough surfaces. *Atmospheric Environment*, *19*, 953–960.

Stapleton, K. W., Guentsch, E., Hoskinson, M. K., & Finlay, W. H. (2000). On the suitability of $k-\varepsilon$ turbulence modeling for aerosol deposition in the mouth and throat: A comparison with experiment. *Journal of Aerosol Science*, *31*, 739–749.

Versteeg, H. K., & Malalasekera, W. (1995). *An introduction to computational fluid dynamics*. Harlow, London: Longman.

Wang, J., & James, P. W. (1999). On the effect of anisotropy on the turbulent dispersion and deposition of small particles. *International Journal of Multiphase Flow*, *25*, 551–558.

Zhang, H., & Ahmadi, G. (2000). Aerosol particle transport and deposition in vertical and horizontal turbulent duct flows. *Journal of Fluid Mechanics*, *406*, 55–80.

Zhang, Y., Finlay, W. H., & Matida, E. A. (2004). Particle deposition measurements and numerical simulation in a highly idealized mouth–throat. *Journal of Aerosol Science*, *37*, 789–803.